Defect trajectories in nematic shells: Role of elastic anisotropy and thickness heterogeneity

David Seč, Teresa Lopez-Leon, Maurizio Nobili, Christophe Blanc, Alberto Fernandez-Nieves, Miha Ravnik, and Slobodan Žumer

Phys. Rev. E **86**, 020705 — Published 29 August 2012

DOI: 10.1103/PhysRevE.86.020705

Defect trajectories in nematic shells: Role of elastic anisotropy and thickness heterogeneity

David Seč,[1] Teresa Lopez-Leon,[2,3,*] Maurizio Nobili,[2,3] Christophe Blanc,[2,3]
Alberto Fernandez-Nieves,[4] Miha Ravnik,[5] and Slobodan Žumer[1,6,7]

[1] *Department of Physics, University of Ljubljana, Jadranska 19, 1000 Ljubljana, Slovenia.*
[2] *Université Montpellier 2, Laboratoire Charles Coulomb UMR5221, F-34095, Montpellier, France.*
[3] *CNRS, Laboratoire Charles Coulomb UMR5221, F-34095, Montpellier, France.*
[4] *School of Physics, Georgia Institute of Technology, 837 State St. NW, 30332 Atlanta, USA.*
[5] *Rudolf Peierls Centre for Theoretical Physics, University of Oxford, Oxford, UK.*
[6] *Jožef Stefan Institute, Jamova 39, 1000 Ljubljana, Slovenia.*
[7] *Center of Excellence NAMASTE, Jamova 39, 1000 Ljubljana, Slovenia.*

We introduce the idea of transformation trajectories to describe the evolution of nematic shells in terms of defect locations and director field when the elastic anisotropy and the shell thickness heterogeneity vary. Experiments are compared to numerical results to clarify the exact role played by these two parameters. We demonstrate that heterogeneity in thickness is a result of a symmetry breaking initiated by buoyancy and enhanced by liquid crystal elasticity, and is irrespective of the elastic anisotropy. In contrast, elastic anisotropy – in particular disfavored bend distortion – drives an asymmetric defect re-organization. These shell states can be both stable or metastable.

PACS numbers: 61.30.Jf, 68.15.+e, 82.70.Kj

Nematic liquid crystal shells offer an interesting way for imprinting well defined interaction sites at a surface using topological defects [1–4]. Controlling the position of the interaction sites - the defects - is not only important from a fundamental point of view but it also determines the directional interactions and the possible structures that can assemble from such ground states [1]. In nematic shells, topological defects arise naturally due to geometrical frustration of the uniaxial three-dimensional nematic order parameter, which is confined between two spherical surfaces. For very thin shells and isotropic elasticity, i.e. equal splay, K_1, and bend, K_3, elastic constants, the tetrahedral symmetry with four topological defects characterizes the ground state [5]. The four defects are of winding number $s = +\frac{1}{2}$, reflecting the π rotation of the average molecular orientation along a path encircling each defect. In infinitely thin shells, the defects become points with two-dimensional topological charge of $+1/2$. For such shells, the sum of four such topological charges is $+2$, as required by the Poincaré and Hopf theorem [6]. By functionalizing these defects, the resultant interactions between shells would emulate the tetrahedral directionality of the sp^3 orbitals of carbon, providing a route for the self-assembly of photonic architectures with tetrahedral symmetry.

The ability to produce shells with other defect configurations would open the routes toward assembling of numerous complex colloidal structures. Experimentally, this has already been achieved by changing the thickness inhomogeneity of shells [2]. Alternatively, using computer simulations on an ideal two-dimensional shell (with zero thickness), the repositioning of the defects was achieved by changing the shape of the shells [7, 8], by exposing them to an external electric field [9] or by introducing elastic anisotropy of the liquid crystal. In particular, for bend energetically much less favorable than splay, the four characteristic $+1/2$ defects are expected to organize themselves along a great circle on a two-dimensional shell [10, 11]. Such defect configuration was recently reported in two independent experimental papers [12, 13], for a temperature sufficiently close to the nematic-to-smectic-A (N-SmA) phase transition, where the elastic constants and the ratio K_3/K_1 are known to increase [14]. In contrast to what was predicted for ideal bidimensional shells, this state is achieved after a series of transformations where the defects follow complex trajectories. Two plausible scenarios were proposed to explain this transition. In the first one, the defects motion would be primarily induced by a change in the geometry of the shell, with the shell becoming more homogeneous in thickness [12]. In the second scenario, the shell would remain heterogeneous and the defect motion would merely result from a change in the elastic constants asymmetry [13]. However, the exact origin of this transformation has not been established yet.

In this paper, we complement experiments with Landau-de Gennes modeling, and study the roles of the shell thickness, its inhomogeneity, and the elastic anisotropy K_3/K_1. We show that multiple (meta)stable director and defect shell states emerge, as achieved by driving the system along distinct transformation trajectories. A progressive increase of elastic anisotropy results in asymmetric shifts of the defect pairs, whereas, a decrease of thickness inhomogeneity gives roughly symmetric shifts. Interestingly, free energy calculations show that inhomogeneous thickness with lost tetrahedral symmetry is inherently favored by the effective nematic elasticity irrespective of the elastic anisotropy. Finally, the

recently observed repositioning of the defects in nematic close to the N-SmA transition is shown to be leadingly determined by the changes in the elasticity anisotropy.

The experimental shells consist of double emulsions produced in a microfluidic device [4]. The middle fluid is a nematic liquid crystal, either 4'pentyl-4-cyanobiphenyl (5CB) or 4-octyl 4'-cyano biphenyl (8CB). The inner and outer fluids are aqueous solutions that contain 1% wt of polyvinyl alcohol (PVA) which enforces planar anchoring of the liquid crystal at the two interfaces. The typical nematic shells have four defect line segments of winding number $s = +\frac{1}{2}$, as shown in Fig. 1(a). These defects are confined to the thinnest part of the shell. The shells are indeed heterogeneous in thickness: the center of the inner drop is typically shifted by Δ with respect to the center of the outer drop [inset to Fig. 1(b)]. The average thickness, h, is given by the difference between the outer and inner radii, $h = R - a$. In our experiments, R is in the range of $(30 - 120)\mu$m and h is $(2\% - 3\%)$ of R.

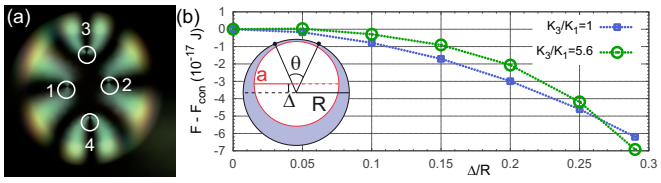

FIG. 1. (a) Top view of an inhomogeneous nematic shell between crossed polarizers. The four $s = \frac{1}{2}$ defects are localized at the thinnest region. (b) Free energy difference between the inhomogeneous and the concentric shell, $F - F_{con}$, as a function of eccentricity Δ/R for $K_3/K_1 = 1$ and $K_3/K_1 = 5.6$. Inset shows schematic side view of a shell, with defect pairs sustaining a relative angle θ.

Both buoyancy effects (due to density mismatch) and elastic forces are expected to contribute to the thickness heterogeneity and the confinement of defects. To determine the role of elasticity, we computed the equilibrium free energy of weightless shells. The simulations were done using minimization of the phenomenological Landau-de-Gennes free energy based on the tensorial order parameter Q_{ij} [15]: $F = \int_{LC} (f_{el} + f_L)\, dV + \int_S f_S dS$, where f_{el} is the elastic free energy density [16]:

$$f_{el} = \frac{L_1}{2} Q_{ij,k} Q_{ij,k} + \frac{L_2}{2} Q_{ij,j} Q_{ik,k} + \frac{L_3}{2} Q_{ij} Q_{kl,i} Q_{kl,j}, \quad (1)$$

with $Q_{ij,k}$ the derivative of the ij-th component of the Q tensor with respect to the Cartesian coordinate x_k, and L_1, L_2 and L_3 the tensorial elastic constants, which map to the standard Frank-Oseen elastic constants K_i as: $K_1 = \frac{9}{4} S^2 (2L_1 + L_2 - L_3 S)$, $K_2 = \frac{9}{4} S^2 (2L_1 - L_3 S)$, and $K_3 = \frac{9}{4} S^2 (2L_1 + L_2 + 2L_3 S)$ [17]. The free energy density f_L accounts for the variation of nematic order $f_L = \frac{A}{2} Q_{ij} Q_{ij} + \frac{B}{3} Q_{ij} Q_{jk} Q_{ki} + \frac{C}{4} (Q_{ij} Q_{ij})^2$, where A, B, and C are the nematic material parameters. The surface free energy density f_s characterizes the planar-degenerate anchoring at the outer and inner surfaces of the shell: $f_s = W(\tilde{Q}_{ij} - \tilde{Q}^{\perp}_{ij})^2$ where W is the anchoring strength, $\tilde{Q}$ and $\tilde{Q}^{\perp}$ are related to the full order parameter tensor, as defined in [18].

We minimize the total free energy numerically by using an explicit Euler relaxation finite difference scheme [19]. The shells are modeled as closed spherical simulation layers of mesh points, cut-out from a uniform cubic grid with resolution δ, which has to be chosen appropriately to avoid pinning of the defects. Due to the coarseness of the shell surface on the cubic grid, the *absolute* values of the total free energy are calculated within $5 - 10\%$ precision; however, free energy differences of higher precision ($\sim 0.01\%$) can be attained if performing calculations at the same allocation of the shell within the mesh. Being only interested in the equilibrium configurations, the effects of the fluid flow are neglected. The initial conditions for the relaxation algorithm are typically set as random spins at each mesh point inside the simulation layer. The following numerical parameters are used in simulations if not stated differently: $R = 2\mu$m, $a/R \lesssim 0.95$, $h \geq 10\delta$, $K_1 = K_2 = K_3 = 51$ pN (for anisotropic elasticity K_3 was increased); $A = -0.172$ MJ/m^3, $B = -2.12$ MJ/m^3 and $C = 1.73$ MJ/m^3; and $W = 5 \times 10^{-3}$J/m^2. These values approximately correspond to 5CB under strong planar degenerate anchoring [20]; thus the effects of splay-bend K_{24} are neglected.

To understand the evolution of the shell states via different transformation trajectories we first analyze the effects of shell inhomogeneity and the elastic constant anisotropy on the defect positions in stable shell states. We examine shells with fixed average thickness h, but varying shift Δ. The difference between the total free energy $F(\Delta)$ of a heterogeneous shell and the free energy $F_{con} = F(0)$ of the corresponding concentric shell is computed for isotropic elastic constants, $K_3 = K_1$, and for a given anisotropy $K_3/K_1 > 1$. A typical result is given in Fig. 1(b) for a simulated shell of thickness $h = 0.3R$. Interestingly, we find that $F(\Delta) - F_{con}$ is negative in both situations, which indicates that heterogeneous shells ($\Delta \neq 0$) are always lower in energy, even when neglecting gravity. Buoyancy, which breaks the symmetry at $\Delta = 0$, enhances this tendency and favors vertical shifts. For this reason, we only observe two possible configurations with the inner drop shifted up or down in the vertical axis, depending on the relative density of the inner drop with respect to the outer one.

Although simulations show that the shift Δ tends to become maximal, the inner and outer surfaces of experimental shells are not observed to coalesce. This reveals the existence of a disjoining pressure, probably due to the presence of PVA, which increases as the nematic film gets thinner and tends to homogenize the thickness. In thick shells, the defects localize at the thinnest region; the ground state is well reproduced by simulations, as shown in Fig. 2(a,d) for $h = 0.1R$, $\Delta = 0.08R \approx h$, and

$K_3/K_1 = 1$. The director field connects the defects by pairs: the two closest defects, 1 and 2 in Fig. 2(d), are connected by a director field that runs along the shortest arc, whereas the defects 3 and 4 are connected by the longest arc spanning a large fraction of a great circle. When reducing Δ, the defects increase their separation in a roughly symmetrical way, as shown in Fig. 2(e,f), i.e. the ratio between the 1-2 and 3-4 defect pair distances remains roughly constant. This is in nice agreement with experiments when osmosis [2] is used to swell the inner drop and decrease h, as shown in Fig.2(b,c).

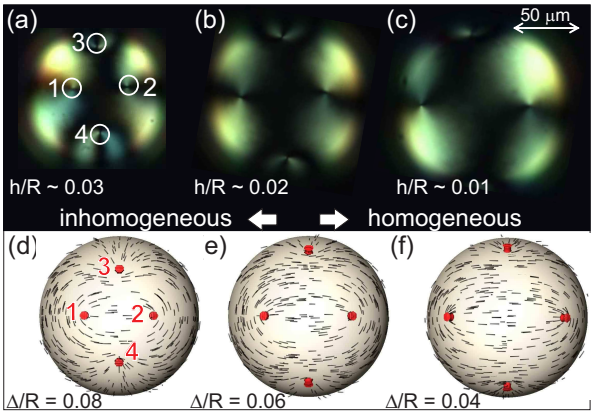

FIG. 2. $(a-c)$ Experimental cross polarized micrographs of three different shells with similar size but different average thicknesses h, and $(d-f)$ corresponding simulated structures. The director is shown in black; defects are drawn in red as isosurfaces of nematic degree of order $S = 0.48$.

Concomitantly with thickness heterogeneity, the elastic constant anisotropy K_3/K_1 also affects the position of the defects. To study their intertwined role, we have simulated inhomogenous thick shells of fixed geometry ($\Delta = cst. \approx h$) and increased K_3. Even at relatively small anisotropy $K_3/K_1 \approx 1.8$, the four defects organize in an asymmetric configuration, with the angular distance between defects 1 and 2, θ_{12}, larger than the angular distance between defects 3 and 4, θ_{34}, as shown in Fig. 3(a,d). Increasing K_3/K_1 further enhances this asymmetry, as shown in Fig. 3(b,e) and Fig. 3(c,f). Defects 1 and 2 move towards opposite sides of the sphere - θ_{12} increases - until they stabilize in the equatorial plane for $K_3/K_1 = 5.6$. Up to this value, defects 3 and 4 do not shift - θ_{34} barely changes. If selectively functionalized, the defects 1 and 2, in this large elastic anisotropy ground state ($\theta_{12} \approx 180°$), could emulate the linear sp orbitals of carbon. A selective functionalization could be simplified by the fact that defects 3 and 4 are much shorter than defects 1 and 2. Upon further increasing the elastic anisotropy, $K_3/K_1 > 5.6$, defects 3 and 4 progressively migrate towards the equatorial plane - θ_{34} increases. The migration of the two defect pairs occurs along two orthogonal great circles, so that, in the final state, the four defects are located at the vertices of a square on the equatorial plane. This final state coincides with the configuration predicted for an ideal bidimensional shell [10, 11].

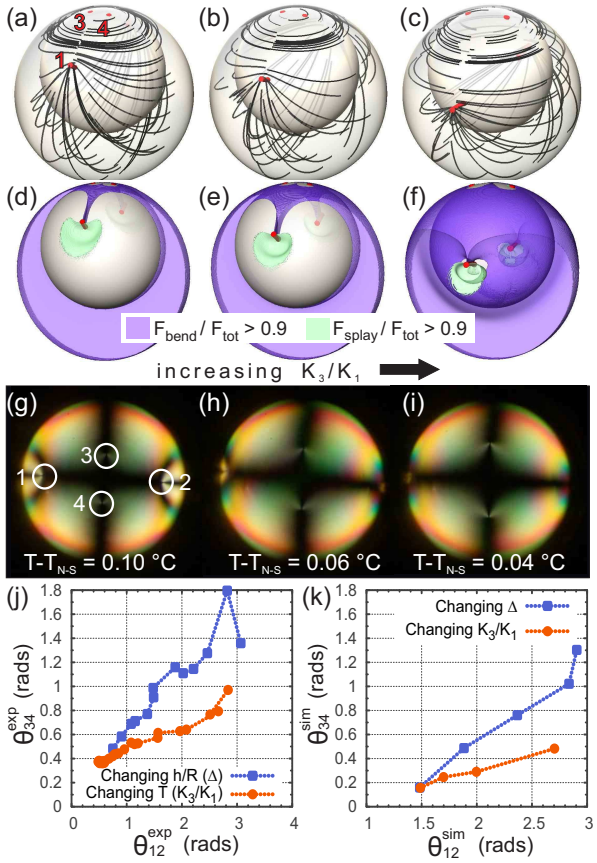

FIG. 3. Increasing elastic anisotropy K_3/K_1 in an inhomogeneously thick shell. (a-c) Side views of simulated shells with varying elastic anisotropy: $K_3/K_1 = 1.8$, $K_3/K_1 = 2.5$, $K_3/K_1 = 5.6$, and fixed $\Delta/R = 0.29$; (d-f) Regions of leading bend (in purple) and splay distortions (in green). Note, the increase of bend at the top thinner part of the shells. (g-i) Micrographs of experimental repositioning of the defects by decreasing temperature T by approaching nematic-smectic phase transition T_{N-S}, i.e effectively changing K_3/K_1. The equilibrium angular distances between defects (red circles in experiments (j) and simulations (k)) behaves differently than when the shell thickness become inhomogeneous (blue squares); note, how defects follow elementary different routes.

The origin of the observed asymmetry in the repositioning of the defect pairs is revealed by calculating the bend and splay elastic contributions to the total free energy. The defects rearrangement towards the equatorial plane results in longer defect cores, but it also provokes a re-distribution of the areas where distortions are mostly bend so that the total free energy decreases. On a sphere, bend distortion is minimal when the director is along great circles. As a result, bend distortions can be quantified using the geodesic curvature of the director field lines that measures any deviation from a great circle. As θ_{12} increases due to an increase in the elastic anisotropy, re-

gions of high geodesic curvature localize to the effectively thinnest region of the shell, while regions of low geodesic curvature localize to the effectively thicker region of the shell, as shown in Fig. 3(a-c). Indeed, calculating the local bend or splay elastic free energy density, shows that the distortion becomes leadingly bend in the thinner region of the shell [increased purple region at the top in Figs. 3(d-f)] as defects 1 and 2 move to the equator.

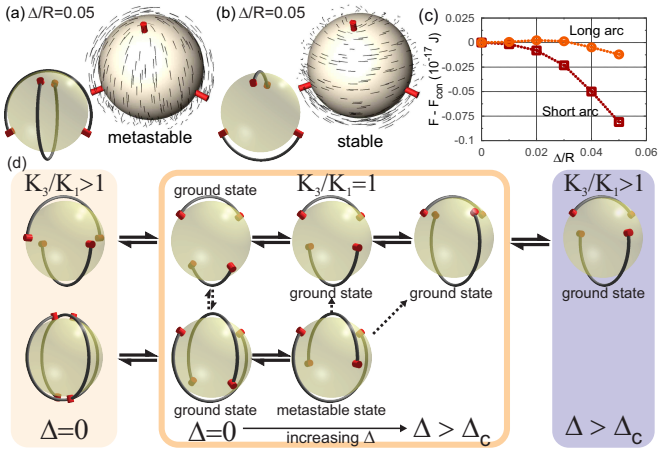

FIG. 4. (a) Metastable and (b) stable inhomogeneous shell states with equal defect positions and non-equal director: the director links defects over the long and over the short arc (see black lines in schematics). (c) Free energy difference between the states in (a) and (b). (d) Scheme of transformation trajectories between -director and defect- shell states that can be controlled by varying inhomogeneity Δ and elastic constant anisotropy K_3/K_1. Note transitions (dashed arrows) and hysteresis in trajectories. The metastable state becomes unstable at Δ_c that may depend substantially on R and h.

Either varying Δ or K_3/K_1 induces rearrangements of defects; however, the way they reorganize is very different. We note that, in the experiments reported in Refs [12, 13], the shell is cooled down near the SmA phase where K_3 increases substantially. Experimentally, the defects migrate to the equatorial plane in an asymmetric way [Figs. 3(g-i)] that closely matches the simulation results of Fig. 3. This confirms that the motion is primarily driven by the increase of K_3/K_1 rather than by the inhomogeneous decrease of the thickness. The different behaviors shown in Fig. 2 and Fig. 3 are easily distinguished by plotting the evolution of θ_{34} with θ_{12}. Figures 3(j,k) summarize the trends observed both in experiment and in simulations. The angular distance θ_{34} increases faster with θ_{12} when varying Δ (squares) than when varying K_3/K_1 (circles). Typically, the errors of experimental data is under $\sim 2\%$.

Note finally that different director (meta)stable states and defect positions could be achieved by gradually tuning the elastic constant anisotropy and the thickness inhomogeneity (Fig. 4). In shells with inhomogeneous thickness, the simulations indeed predict a novel metastable state [see Fig. 4(a) for $\Delta/R = 0.05$] in addition to the ground state [Fig. 4(b)]. These states have distinctly different director fields but identical defect locations. In the stable configuration, the defects are connected along short arcs, whereas they are connected along long arcs in the metastable structure. Free energy difference between the two structures is typically $\sim 1\%$ for 1 μm shells and $\Delta/R = 0.05$ [Fig. 4(c)]. Both stable and metastable inhomogeneous (homogeneous) states belong to the same symmetry group C_2 (D_2). The evolution with Δ and K_3/K_1 is schematically represented in Fig. 4(d). The two states are energetically equivalent for $\Delta = 0$ and $K_1 = K_3$. The duality is broken upon increasing Δ as the defects reposition to the thinner region of the shell. In simulations, the stable state is commonly obtained after a thermal quench, whereas the metastable state can be obtained by gradually increasing Δ (white background) until it becomes unstable at $\Delta_c/R \approx 0.1$ for 1 μm shells. The case of large thickness inhomogeneity and elastic anisotropy (purple background) has been investigated in detail throughout the paper. Interestingly, we predict a new phenomenon when keeping the shell homogeneous in thickness and increasing the elastic constant anisotropy [yellow background in Fig. 4(d)]. In this case, the director arcs of both states (of nearly same energy) become longer, yet driving strongly different repositioning of the defects: either to the equator or to the poles. More generally, this indicates the importance of the transformation trajectories when controlling or generating various states in systems with effectively reduced dimensionality like nematic shells.

We have shown that anisotropy in the elastic constants induces changes in the defect configuration that are very different from the changes when the shell inhomogeneity is changed. By changing the ratio of bend to splay elastic constants, the position of the defects changes in a asymmetric way, whereas by changing the inhomogeneity of the shells, the all four defects reposition roughly symmetrically. Interestingly, the nematic elasticity always prefers the non-homogenic configuration of the shells, which permits repositioning of the defects in different ways. Combining both effects provides a route for controlling distinct defect trajectories that could lead either to same or different topological stable or metastable states. Such writing onto a shell by controlling defect trajectories opens a new functionality of liquid crystal shells. Finally, the intercalation of tunable elastic anisotropy, variable shell homogeneity, and buoyancy could eventually be exploited to fabricate particles with new binding directionalities.

T.L-L. thanks the EU MC Program IEF-236091; A.F-N. thanks NSF DMR-0847304; M.R. acknowledges EU MC Program ACTOIDS; D.S. and S.Ž. acknowledge ARRS program P1-0099 and EU ITN HIERARCHY.

* Teresa.Lopez-Leon@univ-montp2.fr

[1] D. R. Nelson, Nano Letters **2**, 1125 (2002).
[2] T. Lopez-Leon et al, Nat. Phys. **7**, 391 (2011).
[3] T. Lopez-Leon and A. Fernandez-Nieves, Colloid. Polym. Sci. **289**, 345 (2011).
[4] A. Fernandez-Nieves et al, Phys. Rev. Lett. **99**, 157801 (2008).
[5] T. C. Lubensky and J. Prost, J. Phys. II **2**, 371 (1992).
[6] H. Poincaré, J. Math. Pures Appl. **1**, 167 (1885).
[7] M. A. Bates et al, Soft Matter **6**, 655 (2010).
[8] S. Kralj et al, Soft Matter **7**, 670 (2011).
[9] G. Skačej and C. Zannoni, Phys. Rev. Lett. **100**, 197802 (2008).
[10] H. Shin et al, Phys. Rev. Lett. **101**, 037802 (2008).
[11] M. A. Bates, J. Chem. Phys. **128**, 104707 (2008).
[12] H.-L. Liang et al, Phys. Rev. Lett. **106**, 247801 (2011).
[13] T. Lopez-Leon et al, Phys. Rev. Lett. **106**, 247802 (2011).
[14] N. V. Madhusudana and R. Pratibha, Mol. Cryst. Liq. Cryst. **89**, 249 (1982).
[15] P. G. de Gennes and J. Prost, *The Physics of Liquid Crystals*, 2nd Ed. (Oxford, 1993).
[16] M. K. McCamley et al, Appl. Phys. Lett. **91**, 141916 (2007).
[17] K. Schiele and S. Trimper, Pyhs. Stat. Sol. B **118**, 267 (1983).
[18] J.-B. Fournier and P. Galatola, Europhys. Lett. **72**, 403 (2005).
[19] M. Ravnik and S. Žumer, Liq. Cryst. **36**, 1201 (2009).
[20] H. J. Coles, Mol. Cryst. Liq. Cryst. **49**, 67 (1978).